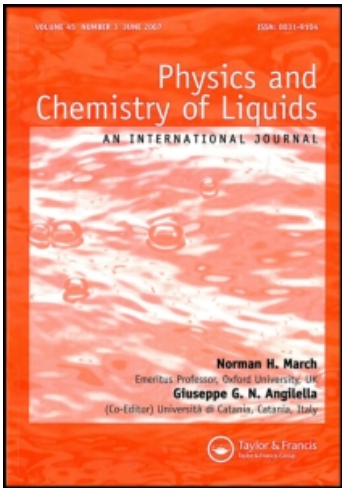

Physics and Chemistry of Liquids
Publication details, including instructions for authors and subscription information:
http://www.informaworld.com/smpp/title~content=t713646857

Brownian Dynamics Simulations of Aggregation and Gel Formation in Lennard-Jones Fluids

J. F. M. Lodge[a]; D. M. Heyes[a]
[a] Department of Chemistry, University of Surrey, Guildford

To cite this Article Lodge, J. F. M. and Heyes, D. M.(1996) 'Brownian Dynamics Simulations of Aggregation and Gel Formation in Lennard-Jones Fluids', Physics and Chemistry of Liquids, 31: 4, 209 — 230
To link to this Article: DOI: 10.1080/00319109608031656
URL: http://dx.doi.org/10.1080/00319109608031656

Phys. Chem. Liq., 1996, Vol. 31, pp. 209–230
Reprints available directly from the publisher
Photocopying permitted by license only

BROWNIAN DYNAMICS SIMULATIONS OF AGGREGATION AND GEL FORMATION IN LENNARD-JONES FLUIDS

J. F. M. LODGE and D. M. HEYES

Department of Chemistry, University of Surrey, Guildford, GU2 5XH

(Received 5 November 1995)

We report structural, thermodynamic and rheological properties of a three dimensional Lennard-Jones fluid as it is quenched, at various densities, from above the critical temperature into the two phase gas-liquid coexistence region. The structural and dynamical behaviour observed has many similarities with a sol-gel transition. There is a growth in cluster size for the spherical particles, evident also in growing peak heights in the radial distribution function, with the formation of a percolating network at low temperature ($T \sim 0.2$–0.3) and at sufficiently high volume fractions (> 0.1). This change is also marked by diverging structural relaxation times, manifest in an increasing viscosity and decreasing self-diffusion coefficient during the quench. The shear stress time correlation functions exhibit stretched exponential behaviour at long time. In fact, limiting long time relaxation is dominated by a single relaxation time, which is evident in excellent Maxwell-like viscoelastic behaviour in the low frequency region of the dynamic moduli.

KEY WORDS: Sol-gel transition, 3D Lennard-Jones, spinodal decomposition, Brownian dynamics, computer simulation.

1 INTRODUCTION

Aggregation of colloidal particles has been the subject of many experimental and theoretical studies in recent years. The cluster that grow form a self-similar structure that was first noted by Vold[1] and subsequently characterized in terms of the fractal dimension, D_f. The mechanism of growth determines the fractal dimension of the clusters, as has been elegantly shown using lattice computer simulation techniques[2,3]. The fractal dimension of clusters for gold, silica and polystyrene particles, has been found to be $D_f = 1.75$ for fast aggregation and $D_f = 2.02$–2.12 for slow aggregation[4]. At sufficiently large volume fraction, an infinitely spanning network or 'gel' forms from the clusters as they merge together to form a connected cluster of macroscopic dimension (this is known as the sol-gel transition–sol referring to a state with finite sized clusters). These so-called 'particle' gels (as distinct from polymer gels) form a useful model for a range of soft solid-like foods including yoghurt and cheese.

The gel point, GP, is a second order transition in connectivity, which is characterised by a divergence in the viscosity beneath the GP and a growth of the elastic modulus, G above the gel point. Near the sol-gel transition, gelling systems exhibit a slowing down in structural relaxation as a result of the divergence in average cluster

size. For example, for the viscoelastic behaviour, as the gel point is approached, correlation functions become more nonexponential, reflecting an increasingly broad range of relaxation times. The correlation function has been found to be initially a power law decay, $\sim t^{-\alpha}$, terminating in a stretched exponential, $\sim \exp(-t/\tau)^{-\beta}$), with $\beta \sim D_f/(D_f+1)$[5,6,7,9,12]. Before the gel point the stress correlation function is truncated by a stretched exponential, beyond a certain (divergent) time. At the gel point, the decay is power law[7,8]. The viscoelastic behaviour of physical ('entanglement') and chemical (e.g., silica) gelling systems near the sol-gel transition manifest a power law decay with time of the stress relaxation function and the dynamic moduli, $G'(\omega), G''(\omega) \propto \omega^{\Delta}$[13,9,10]. A consequence of this scaling is that $\tan(\delta) = G''/G'$ is independent of frequency, which has been convincingly demonstrated in a number of recent experimental studies on crosslinking gels[9,11,13]. This behaviour has however still to be observed for the particle gels. Well above GP, for particle gels, the elastic modulus increases as ϕ^{γ}, where ϕ is the solids volume fraction, where γ lies in the range 3.7–4.5 from different studies[14,15].

Recent studies of polymer induced flocculation by the depletion mechanism and gelation of monodisperse spherical colloidal particles located the gel state in the two-phase coexistence region[16,17]. As the system is 'quenched' into the two phase region (by adding free non- adsorbing polymer) a gel state can be formed. There still remain unresolved fundamental issues relating to gel formation in attractive particle systems. For example the effect of particle concentration and strength of attraction between the particles on the level and nature of clustering, and the effects these have on the dynamic rheology of these systems around the gel point. Further work is required to establish the relationship between the equilibrium phase diagram and viscoelastic behaviour. The purpose of the present study is to a) explore if it is possible to model the process of gel formation by Brownian dynamics and b) to attempt to resolve some of the above issues using this method. A 3D Lennard-Jones model is employed, because its phase diagram is now known very well, and its form is not unrealistic for some colloidal systems.

The LJ phase diagram is given in Figure 1), based on recent co-existence data[18,19]. The curves delimit various regions in the T vs. ρ plane. Outside the gas-liquid coexistence line, either the gas, liquid or fluid phases are stable. However, inside the gas-liquid coexistence line a single phase gas or liquid is not at thermodynamic equilibrium. The gas and liquid phases co-exist. Approaching from left to right on the figure, in the metastable region growth of the liquid phase proceeds by nucleation ('germination') and accretion of the gas molecules onto the surface of the clusters. In the unstable region, density fluctuations on all wavelengths are facile, and the development of two phases takes place by a process known as 'spinodal decomposition'. The spinodal line shown on the figure was estimated from the locus of $(\partial P/\partial \rho)_T = 0$ in the two phase region, using a recent Lennard-Jones parameterised equation of state[20]. Simulation studies of 2D Lennard-Jones fluids have been carried out and demonstrated this growth mechanism[21,22] for a single component fluid and also for a 2D binary fluid[23]. An earlier study of spinodal decomposition in 3D LJ single component fluids is given in Ref. [24].

The spinodal region is something of a transient curiosity in molecular fluids, as the time scales are rather short ($\tau \sim 10^{-9}$S). However, in colloidal systems, the relaxation

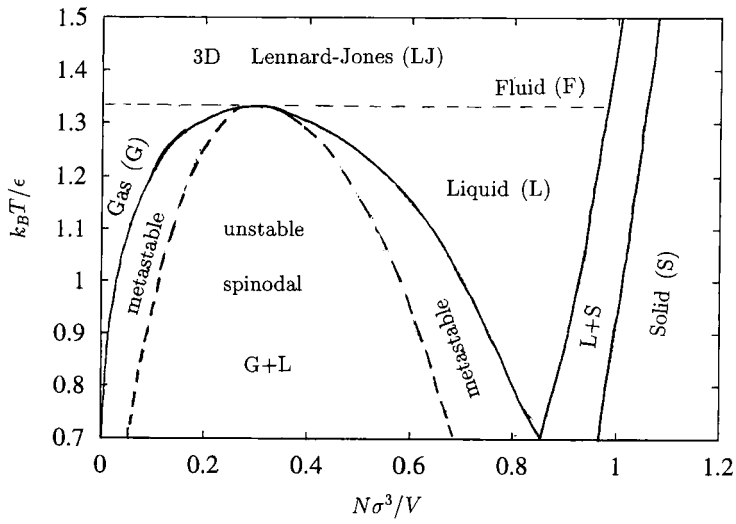

Figure 1 The Lennard-Jones phase diagram.

times scale as the cube of the particle diameter and the solvent viscosity, so that this transient process is long and is significant on human time-scales. The relaxation times can be years, so that the early stages of the spinodal process in these systems, where there is still a percolating network, called a gel, is of considerable practical importance not least in the area of consumer health-care and cosmetic products.

2 COMPUTATIONAL DETAILS

We consider a cubic simulation cell containing N LJ model molecules. The volume fraction, $\phi = \pi N\sigma^3/V$, where V is the volume of the simulation cell, is V. The volume fractions chosen for our simulations are $\phi = 0.030, 0.100, 0.150, 0.300, 0.31416, 0.455$ and 0.500. In each case an equilibrated system above the critical temperature, was quenched in stages down in temperature well into the two phase region. Recent critical point values for the truncated LJ molecule are, $T_c = 1.321 \pm 0.004$ and $\rho_c = 0.306 \pm 0.001$ [18]. Calculated properties are quoted in particle based reduced units, e.g., σ for length, ε for energy, and $\sigma(m/\varepsilon)^{1/2}$ for time, where m is the mass of the model colloid particle. The Brownian Dynamics simulation technique is the same as we have used in previous studies (e.g.,[27]).

The Lennard-Jones potential is used to represent the interaction between model colloidal particles in the simulation,

$$\phi(r) = 4\varepsilon\left(\left(\frac{\sigma}{r}\right)^{12} - \left(\frac{\sigma}{r}\right)^{6}\right) \tag{1}$$

substituted in the Zwanzig-Mountain formula for the shear rigidity modulus at infinite frequency, G_∞ [25] gives

$$G_\infty = \rho(108\langle u_{12}\rangle - 18\langle u_6\rangle)/15 \tag{2}$$

where $\langle u_{12}\rangle$ and $\langle u_6\rangle$ are the average r^{-12} and r^{-6} interaction energy per particle. In the case of the colloidal systems G_∞ was computed during the simulation as a time average.

The stress tensor, $\underline{\sigma}$, is in terms of the microscopic details,

$$\underline{\sigma} = \frac{\rho}{N}\sum_{i=1}^{N-1}\sum_{j=i+1}^{N}(\underline{r}_{ij}\,\underline{r}_{ij}/r_{ij})\,V'_{ij}. \tag{3}$$

We also compute the shear-stress time autocorrelation function, $C_s(t)$,

$$C_s(t) = \frac{V}{k_B T}\langle \sigma_{xy}(0)\sigma_{xy}(t)\rangle, \tag{4}$$

where $\langle\cdots\rangle$ indicates an average over time origins in Eqn. (4). This is the same as a shear stress relaxation function, as would be measured in a step-in-strain experiment in the limit of zero strain. A useful relationship (and consistency check in the simulation) is

$$G_\infty = C_s(t=0). \tag{5}$$

The interaction part of the shear viscosity is given by,

$$\eta_0 = \int_0^\infty C_s(t)dt. \tag{6}$$

The viscosity is conveniently normalised by the solvent viscosity, η_s.

The time correlation function can also be used to calculate the linear viscoelasticity of the colloidal liquid by Fourier transformation. The complex shear modulus is,

$$G^*(\omega) = G'(\omega) + iG''(\omega), \tag{7}$$

where $G'(\omega)$ is the storage modulus and $G''(\omega)$ is the loss modulus. In terms of the stress time-correlation function we have,

$$G^*(\omega) = i\int_0^\infty C_s(t)\exp(-i\omega t)\omega dt. \tag{8}$$

The Maxwell model for a classical viscoelastic fluid, characterised by a single shear stress relaxation time, τ, gives for the time-correlation function, $C_s(t) = G_\infty \exp(-t/\tau)$ where the relaxation time is given by $\tau = \eta_0/G_\infty$,

$$G'(\omega) = \frac{G_\infty(\omega\tau)^2}{1+(\omega\tau)^2}, \tag{9}$$

and

$$G''(\omega) = \frac{G_\infty(\omega\tau)}{1+(\omega\tau)^2}. \tag{10}$$

The storage modulus increases monotonically with $\omega\tau$ and the loss modulus first increases as $\omega\tau$ increases from 0, then maximises and equals the storage modulus at $\omega\tau = 1$.

It is convenient to render the colloid liquid's viscosity in dimensionless units, by dividing them through by the host liquid's viscosity, to form the *relative* viscosity, $\eta_{r0} = \eta_0/\eta_s$ and $\eta_{r\infty} = \eta_\infty/\eta_s$. The complex dynamic viscosity,

$$\eta^*(\omega) = \eta'(\omega) + i\eta''(\omega) \tag{11}$$

is related to the dynamic shear modulus, $G^*(\omega)$ through $G^*(\omega) = \omega\eta^*(\omega)$. We have,

$$\eta'(\omega) = \eta'(\infty) + \Im\left|i\int_0^\infty C_s(t)\,e^{-i\omega t}dt\right|. \tag{12}$$

and

$$\eta''(\omega) = \Re\left|i\int_0^\infty C_s(t)\,e^{-i\omega t}dt\right|. \tag{13}$$

where $\eta'(\infty) = \eta_\infty$ which is hydrodynamic in origin.

The self-diffusion coefficients were obtained from the force auto-correlation function, generalising the treatment of[26]

$$D(t) = D_0 - \frac{1}{3}\int_0^t (1 - t'/t)\langle(\underline{F}(0)/\zeta(0)).(\underline{F}(t')/\zeta(t'))\rangle dt'. \tag{14}$$

The calculations are conveniently carried out in reduced units appropriate to both the interaction potential and the solvent. The system of units used for computation and presentation of data is discussed in Appendix A.

3 RESULTS AND DISCUSSION

As temperature decreases into the two phase region, there is evident a pronounced change in the local structure. This can be seen in the pair radial distribution function, $g(r)$, which shows a dramatic growth in the height of the first peak, which is evidence of a condensation of the particles into clusters. These clusters grow as temperature decreases, manifest in additonal peaks at $\sigma, 2\sigma \ldots$ for the very lowest temperatures considered ($T < 0.5$). Figure 2 presents radial distribution functions for a series of quenches at volume fractions ranging from 0.03 to 0.5. For example, Figure 2(a) gives the $g(r)$ for $\phi = 0.03$ and $\phi = 0.314$ states at several temperatures. Long-range order grows to about 3σ, but further growth is restricted by the low density of particles. However, at $\phi = 0.15$, shown in Figure 2(b), much longer range structures are evident at $T < 0.3$, indicative of a gel-like state. It is therefore probable that, with a given range of attractive interaction, there is a minimum density of particles required to form a gel. It is interesting that there is a peak in the radial distribution function at $r \sim 1.7$, which suggests some local crystalline structure. This is not surprising, as at these low temperatures we are in the gas-solid coexistence part of the phase diagram. This feature is present at $\phi = 0.314$ (Fig. 2(c)) and also at $\phi = 0.500$ (Fig. 2(d)), the latter state is in the liquid-solid region of the Lennard-Jones phase diagram, and therefore the supercooled states are best referred to as glasses[30].

A typical configuration at $T = 0.5$ and $\phi = 0.1$ in Figure 3 gives some evidence of clustering in the two-phase regime. Visual evidence for the gel-structure was rather disappointing. The human eye appears not to be very effective at noticing long-range order in randomly arranged systems. The long range structuring probably takes the form of evolving transient structures (note that there are not chemical bonds between the particles) which can only be identified using a time-average property, such as the radial distribution function. Another such function is the average cluster size (using the definition that a single particle is in a cluster if it is less than 1.84σ from at least one particle already in the cluster) which also shows clearly the growth of co-existing low and high density phases. The interaction distance used to define the cluster is where the interaction potential has the value $-0.1\,\varepsilon$ at a separation greater than the minimum in the pair potential. Figure 4 shows the average cluster size (i.e., number of particles in a typical cluster) as a function of temperature for a $\phi = 0.03$ state. This quantity increases dramatically for $T < 1.0$. Another time-average property that reflects this process of phase separation is the average interaction energy per particle, u, computed from

$$u = \frac{1}{N} \sum_{i=1}^{N-1} \sum_{j=i+1}^{N} \phi_{ij}. \tag{15}$$

Figure 5 shows $u(T)$ for a series of volume fractions. u decreases with temperature, reflecting the increased level of association that takes place in this part of the phase diagram. There is qualitative difference in the behaviour of the systems in the gel regime ($\phi = 0.03 \rightarrow 0.3$) and those in the glassy regime ($\phi = 0.455 \rightarrow 0.5$). The rate of descent is much more gradual on the glassy part of the phase diagram. Excluded

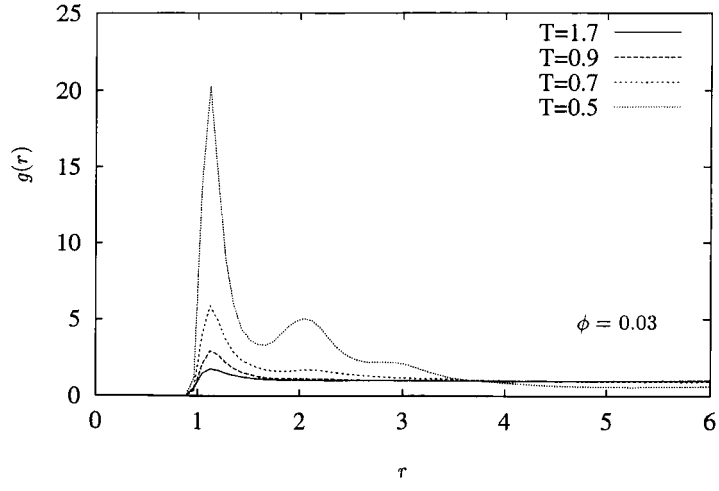

a

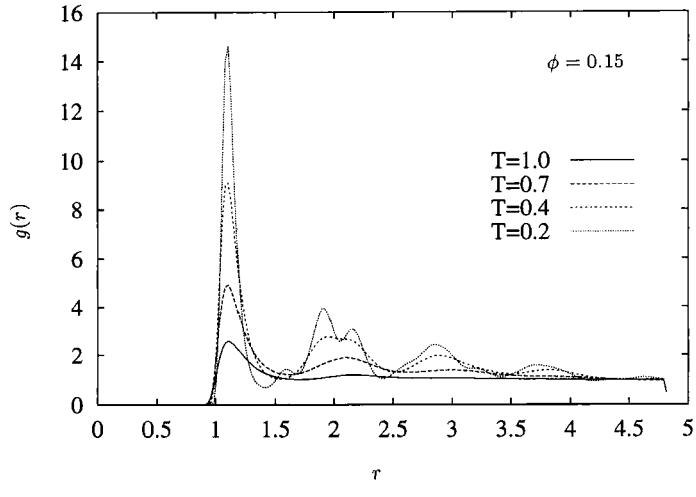

b

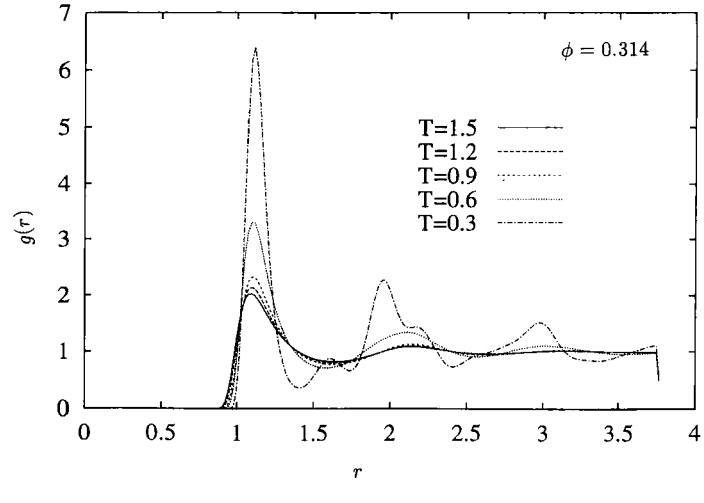

c

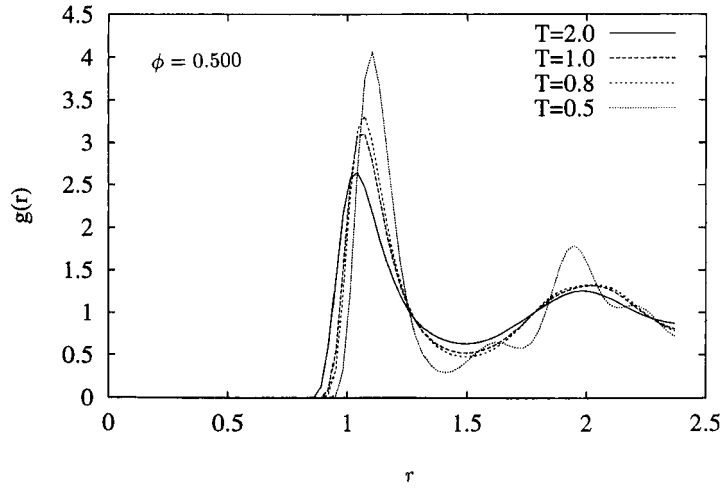

d

Figure 2 Radial distribution functions as a function of temperature given on the figures for: (a) $\phi = 0.03$ and $N = 108$, (b) $\phi = 0.15$ and $N = 256$, (c) $\phi = 0.314$ and $N = 256$, and (d) $\phi = 0.500$ and $N = 108$.

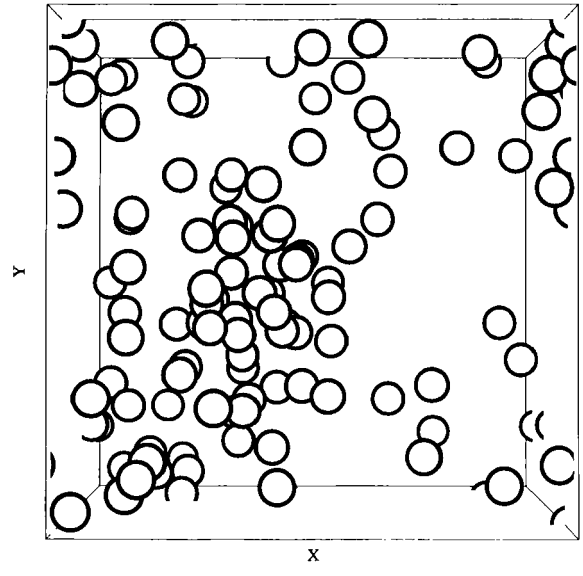

Figure 3 Snapshot configuration in perspective of the LJ particles taken from a $\phi = 0.10$, $T = 0.5$ and $N = 108$ simulation.

volume effects prohibit major structural changes, so there is a limit to the extent that the internal energy can change. However, in the lower density gel regime, structural changes can be much more dramatic owing to the greater free volume. Therefore the transition apparent in u is much sharper than at higher volume fractions, particularly at $\phi = 0.1$, which is clearly close to being an optimum density for gel formation

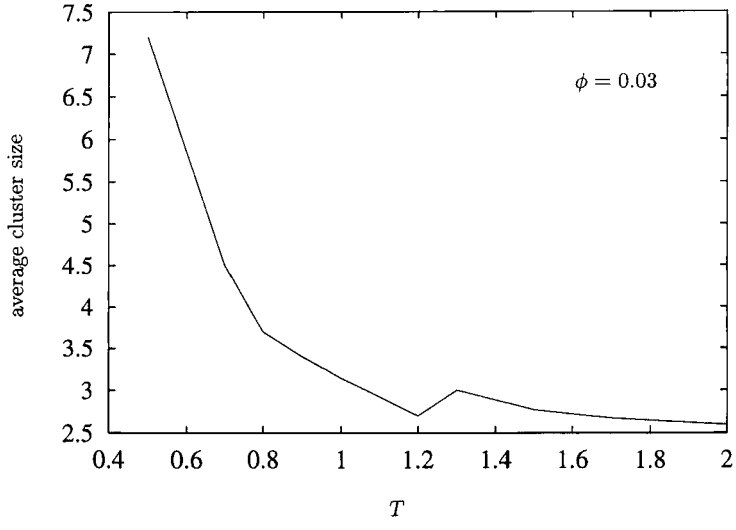

Figure 4 Average cluster size for a $\phi = 0.03$ and $N = 108$ simulation. The search diameter was $r_s = 1.84$.

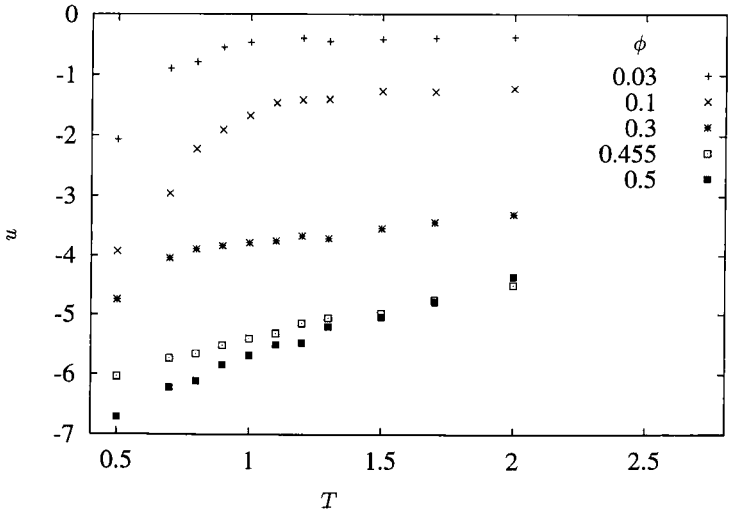

Figure 5 Average interaction energy per particle as a function of temperature for a series of volume fractions, given on the figure ($N = 108$).

with this pair potential. There is a sharp drop in u commencing at $T \sim 1$ as greater morphological changes are possible in this part of the phase diagram. The thermodynamic changes associated with this kinetic transition are much more pronounced that in the glassy region.

The two-phase part of the phase diagram is also characterised by a slowing down in the dynamical behaviour of the molecules. The time dependent diffusion

coefficients, calculated from Eqn. (14) plotted as $D(t)/D_0(T)$ are shown in Figure 6 for $\phi = 0.15$ and $\phi = 0.314$. Note that the self-diffusion coeffcients are normalised by the temperature dependent self-diffusion coefficient at infinite dilution, $D_0(T)$. Therefore we have scaled out the 'trivial' temperature dependent component of the self-diffusion coefficient arising from the variation in the mean square displacements

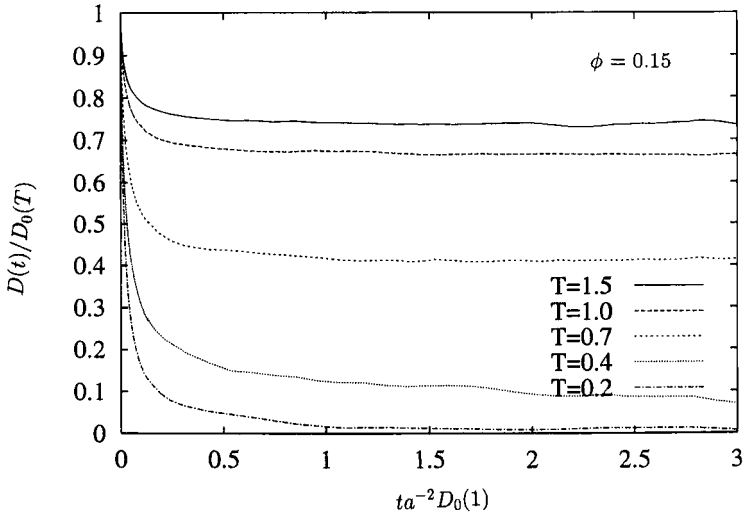

a

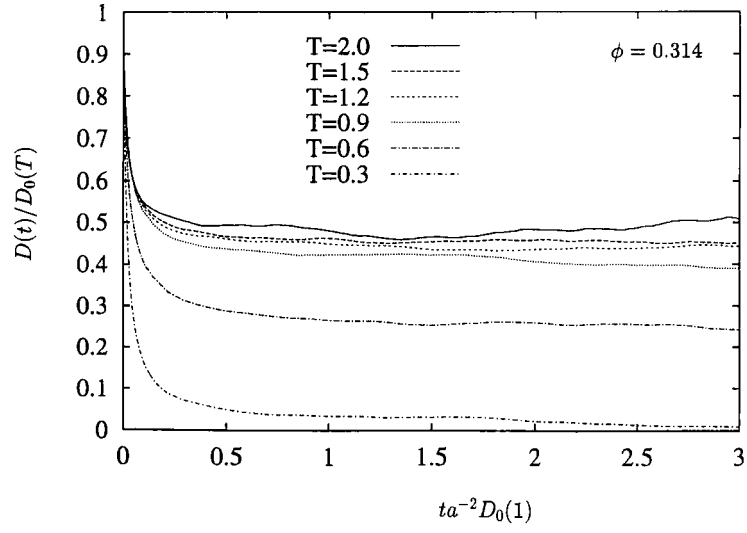

b

Figure 6 Time dependent, diffusion coefficients for (a) $\phi = 0.15$ and (b) $\phi = 0.314$ at temperatures given on the figure.

of the particles. As temperature decreases, the long-time self-diffusion coefficients diminish to smaller values, even after scaling out the trivial temperature dependence. This is reasonable, as the LJ particles increasingly participate in larger agglomerates as temperature decreases and their mobility will be reduced as they take part in the dynamics of larger structural units.

Self-diffusion, being a single particle property, can only give a relatively limited picture of the dynamics of the system. The shear stress autocorrelation function, $C_s(t)$, which is a collective dynamical property shows evidence of a slower decay with decreasing temperature. Figure 7 presents the $C_s(t)$ for the $\phi = 0.15$ and $\phi = 0.314$

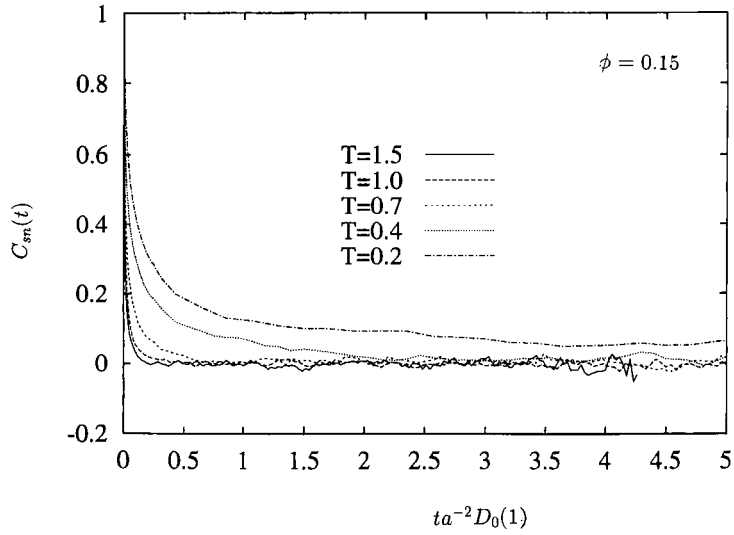

a

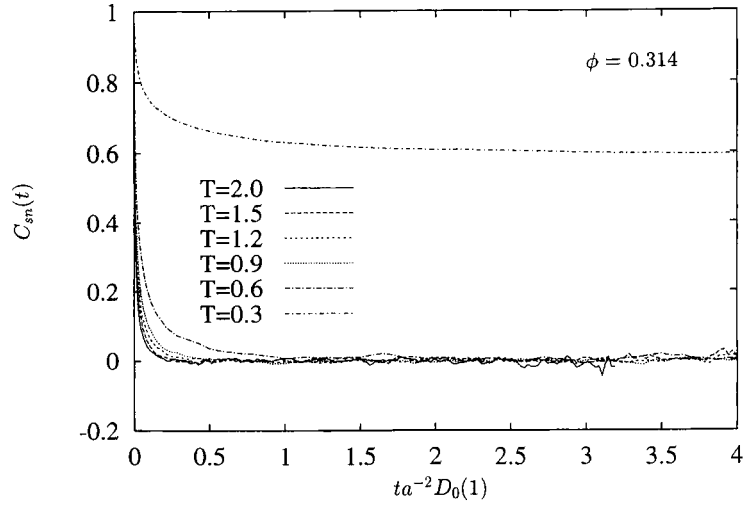

b

Figure 7 Shear stress time correlation functions for (a) $\phi = 0.15$ and (b) $\phi = 0.314$ at temperatures given on the figure.

states. There is a gradual transition for the $\phi = 0.15$ states, with the decay of the correlation function slowing down as temperature decreases. At $\phi = 0.314$ there is a sharp transition at $T = 0.3$, at which point the correlation function decays very slowly (it still has a value of only 0.5 even for the relatively long time $t = 20a^2/D_0(T = 1)$. The long-time self-diffusion coefficient is essentially zero for this state (consult Fig. 6(b)) and therefore we can assume that this state is structurally and kinetically arrested, and has probably gone past the gel-transition to form a highly interconnected network. The gel transition is sharper in the stress correlation function that in $D(t)$, which shows a more gradual evolution through these state. There is a major change in $C_s(t)$ going from $T = 0.6$ to $T = 0.3$, which is not mirrored to the same extent in $D(t)$.

Table 1 presents the thermodynamic quantities and shear rigidity moduli, computed using Eqn. (2) and Eqn. (5), for the $\phi = 0.150$ and 0.314 systems. The two methods for G_∞ agree within statistics for all states apart from $\phi = 0.3142$ and $T = 0.3$, which we have already identified as being well within the gel region. The difference in the two ways of computing G_∞ reflects the non-ergodic nature of this supercooled state. Table 2 gives the corresponding shear viscosities from Eqn. (6) and self-diffusion coefficients calculated using Eqn. (14). The viscosities increase with decreasing temperature, whereas the self-diffusion coefficients diminish with decreasing temperature. The product of the two, also shown in Table 2, indicates that the relative change in viscosity is greater than that of the self-diffusion coefficient. This is reasonable, as one would expect collective properties to reflect to a greater extent the growth in long range connectivity associated with the sol-gel transition. Self-diffusion can still take place to some extent within the percolating framework, especially as these networks are probably evolving in local detail over time, even though the network itself persists over long rheological times.

The temperature dependence of the shear viscosity (Fig. 8) and the shear stress relaxation time, $\tau = \eta_0/G_\infty$ (Fig. 9) show a dramatic increase as temperature decreases. The temperature at which this occurs depends strongly on volume; it

Table 1 Summary of data from the quenched states. Key: ϕ, volume fraction; ρ, number density; T, reduced temperature; u, average interaction energy per particle; P, interaction part of the pressure; G^u_∞, infinite frequency shear rigidity modulus from Eqn. (2); G^c_∞, infinite frequency shear rigidity modulus from Eqn. (5).

ϕ	ρ	T	u	P	G^u_∞	G^c_∞
0.150	0.286	0.2	−5.76	−0.265	7.12	7.14
0.150	0.286	0.4	−5.06	−0.297	6.06	6.14
0.150	0.286	0.7	−3.67	−0.336	4.04	4.08
0.150	0.286	1.0	−2.41	−0.316	2.36	2.37
0.150	0.286	1.5	−1.96	−0.212	2.06	2.10
0.31416	0.600	0.3	−6.28	−1.20	14.46	28.5
0.31416	0.600	0.6	−5.03	−1.15	11.06	11.2
0.31416	0.600	0.9	−4.28	−1.04	9.21	9.23
0.31416	0.600	1.2	−4.10	−0.58	10.06	10.1
0.31416	0.600	1.5	−3.96	−0.14	10.96	11.0
0.31416	0.600	2.0	−3.75	0.55	12.44	12.4

Table 2 As for Table 1, except Key: σ_s, percolation threshold search diameter; η_0/η_s, LJ interaction part relative shear viscosity taken from Eq. (6); $D(T)/D_0(T)$, the reduced long-time self-diffusion coefficient, $D(t \to \infty)$ from Eqn. (14).

ϕ	ρ	T	σ_s	η_0/η_s	$\tau D_0/a^2$	$D(T)/D_0(T)$	$\eta_0 D/D_0\eta_s$
0.150	0.286	0.2	1.0740	14.9	0.890	0.0	0.0
0.150	0.286	0.4	1.0756	4.87	0.341	0.024	0.117
0.150	0.286	0.7	1.1087	1.04	0.109	0.396	0.412
0.150	0.286	1.0	1.1801	0.138	0.025	0.666	0.092
0.150	0.286	1.5	1.2412	0.058	0.012	0.743	0.043
0.31416	0.600	0.3	1.0750	>799	23.44	<0.019	15.0
0.31416	0.600	0.6	1.0780	2.90	0.111	0.237	0.690
0.31416	0.600	0.9	1.0943	0.624	0.029	0.410	0.256
0.31416	0.600	1.2	1.0914	0.646	0.027	0.442	0.286
0.31416	0.600	1.5	1.0882	0.527	0.020	0.457	0.241
0.31416	0.600	2.0	1.0832	0.477	0.016	0.493	0.235

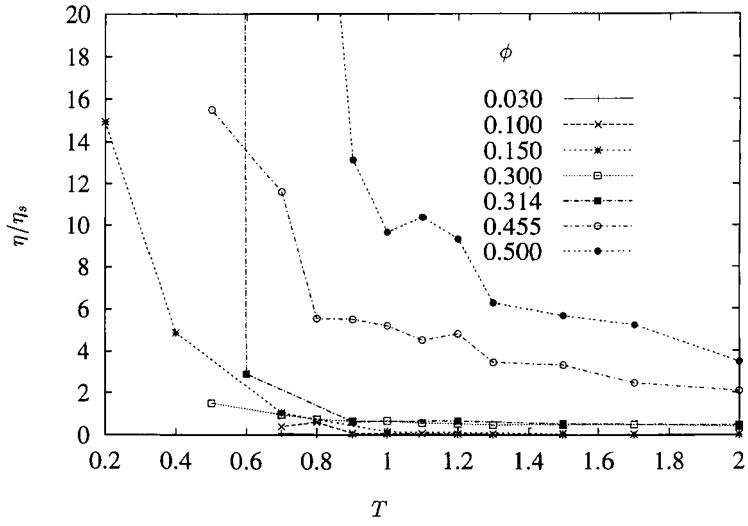

Figure 8 Temperature dependence of the reduced viscosity for a series of volume fractions given on the figure. All simulations were for $N = 108$ except $\phi = 0.150$ and $\phi = 0.314$, which were carried out using $N = 256$.

increases with volume fraction. For $\phi = 0.15$ for example, this occurs at $T \sim 0.5$ whereas for $\phi = 0.455$, the temperature at which divergence starts in $T = \sim 0.9$.

As discussed in the Introduction, the analytic form adopted by the shear stress correlation function is a signature of the onset of gelation that is used in experimental studies (recast as its Fourier transform, $G'(\omega), G''(\omega) \propto \omega^{\Delta}$). With this in mind, we now consider the analytic forms of our computed time correlation functions. In our previous simulations on model stabilised colloidal liquids, using the same algorithm, we found that the computed $C_s(t)$ can be represented very well by a so-called 'fractional' or 'stretched' exponential (except at very short times where this analytic

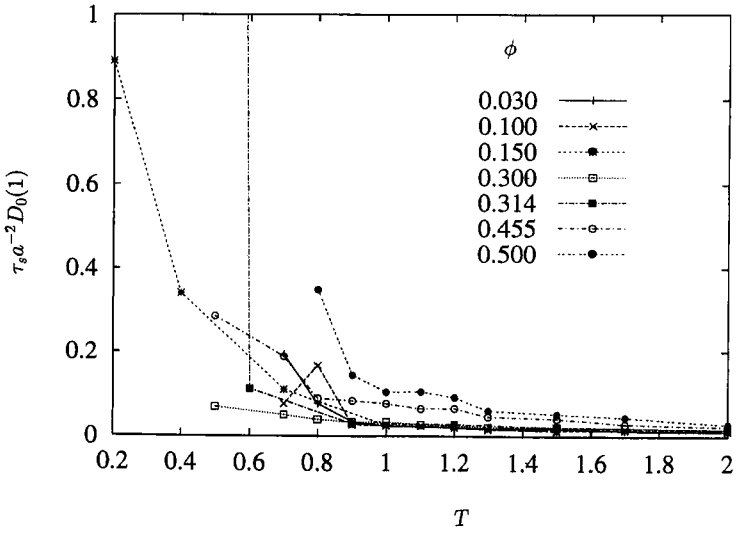

Figure 9 As for Figure 8, except the shear stress relaxation times, τ_s are shown.

form underestimates the simulation $C_s(t)$)[29]. The stretched exponential has the analytic form

$$C_s(t) = G_\infty \exp(-t/\tau')^\beta), \tag{16}$$

where τ' and β are adjustable parameters. A graphical manipulation of the computed **normalised** (i.e., $C_{sn}(0) = 1$) functions is an alternative method for determining the analytic form of the computed BD $C_s(t)$, which has the advantage that adherence to a particular form in only part of the time domain can be readily seen. (The procedure has been suggested previously, e.g.,[28].) For an exponential decay $C_{sn}(t) = \exp(-t/\tau)$, for example, we have that $\ln(C_{sn}(t))$ is linear with slope $-\tau^{-1}$ when plotted against t. For a stretched exponential $\ln(-\ln(C_{sn}(t)))$ has a slope of β and an intercept of $-\beta \ln(\tau')$. An algebraic decay $C_{sn}(t) = At^{-\alpha}$ when plotted as $\ln(C_{sn}(t))$ vs. $\ln(t)$ has a slope of $-\alpha$. Therefore a graphical representation of these computed functions should indicate clearly which of these analytic forms (if any) the data conforms to and in what time regions. Treatment of the computed data revealed that, as for the model stabilised systems, overall the stretched exponential is the analytic form that best describes the data at long time, although this form is not suitable as $t \to 0$. Figure 10, for example, shows a $\ln(-\ln(C_{sn}(t)))$ vs. $\ln(t)$ plot for $N = 108$ and $\phi = 0.3$ systems at a range of temperatures above and in the two-phase region. There is a linear regime at long times for all of the states.

Figure 11 reveals that there is some evidence that the algebraic form is starting to appear in a supercooled state $T = 0.2$, as there is a linear regime $\ln(C_{sn}(t))$ vs. $\ln(t)$. The slope $-\alpha = -1.0$, a little high on the basis of the above fractal dimension criterion. However, at this stage we cannot confirm the generality of this behaviour, as with the current stage-by-stage quench procedure it is difficult to locate the gel point itself, and (**only** at the gel point is algebraic decay thought to dominate).

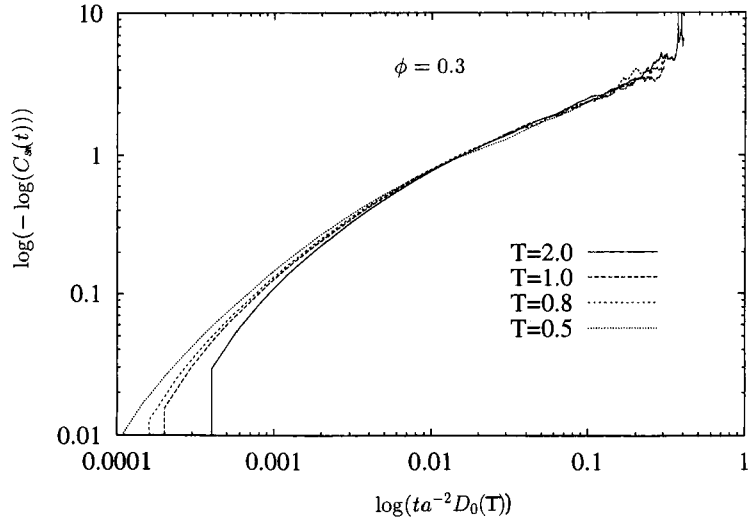

Figure 10 $\log(-C_{sn}(t))$ vs. $\log(t)$ for $\phi = 0.3$ and $N = 108$ at temperatures given on the figure.

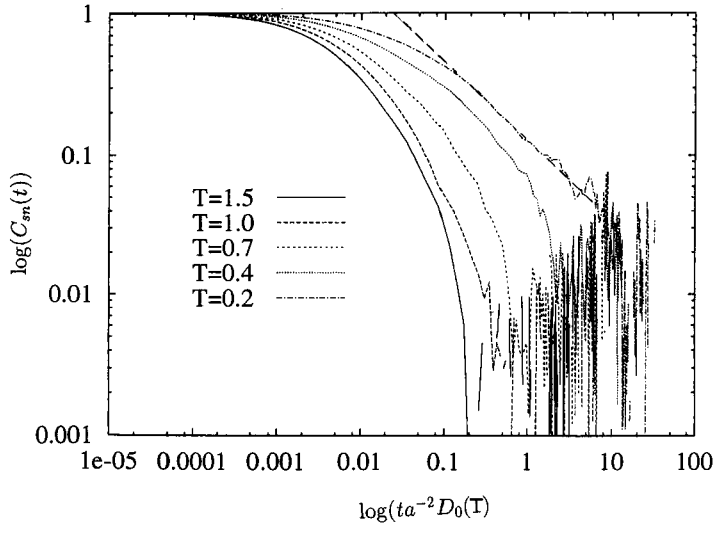

Figure 11 A plot of $\log(C_{sn}(t))$ vs. $\log(t)$ for the $\phi = 0.15$ and $N = 108$ systems.

The storage and loss moduli reveal near-Maxwellian limiting behaviour at low frequency, as illustrated in Figures 12 and 13. The low frequency dynamic moduli at frequencies below $\omega a^2/D_0(1) \sim 5$ can be represented by a single relaxation time Maxwell element. This gives additional support to the conclusion made above, that the stress time correlation function is close to being a stretched exponential at long times. Any stretched exponential can be written as a weighted sum of exponentials

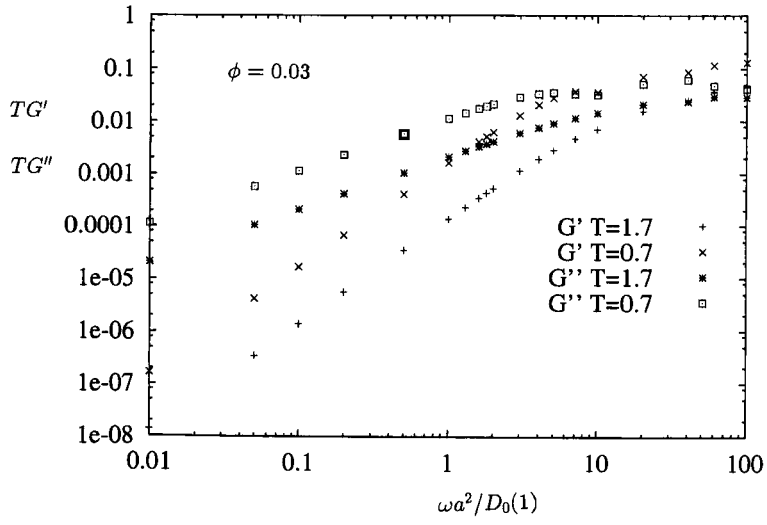

Figure 12 The G' and G'' for $\phi = 0.03$ and $N = 108$. Note the near-linear behaviour at low frequency at temperatures given on the figure.

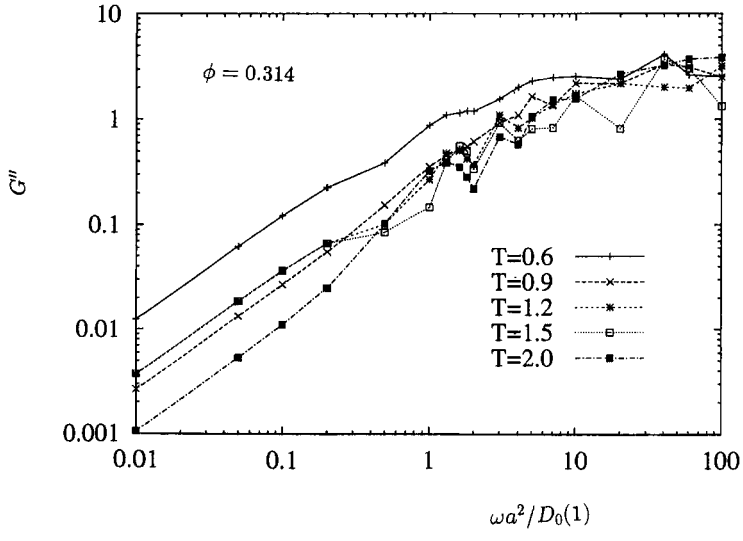

Figure 13 The G'' for $\phi = 0.314$ and $N = 256$ states at temperatures given on the figure.

with different relaxation times. It would appear that at long times only one of these 'Maxwell elements' survives and therefore a single relaxation time, the so-called 'longest relaxation time', τ_1, dominates the evolution of the system on these time scales[33]. This occurrence of a characteristic time at long times is widespread in polymer and colloidal systems. This relaxation time can be computed as a function of frequency from $\tau_1(\omega) = G'/\omega G''$, on assuming Maxwell behaviour to hold at each frequency. Figure 14 shows $\tau_1(\omega, T)$ for the $\phi = 0.314$ states, and reveals that it

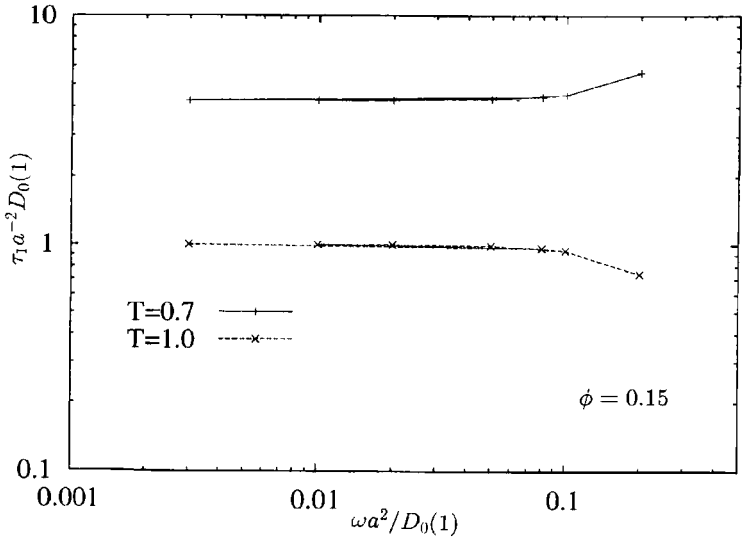

Figure 14 The longest relaxation time τ_1 for the $\phi = 0.15$ and $N = 256$ state as a function of frequency in the low frequency limit.

reaches a constant value, somewhere between a value of $1 - 10a^2 D_0^{-1}(1)$, depending on temperature. The longest relaxation time, τ_1, is observed to increase with diminishing temperature in a similar manner as the mean relaxation times (see Fig. 15), defined earlier from the viscosity, τ_s. The values of τ_1 are typically an order of

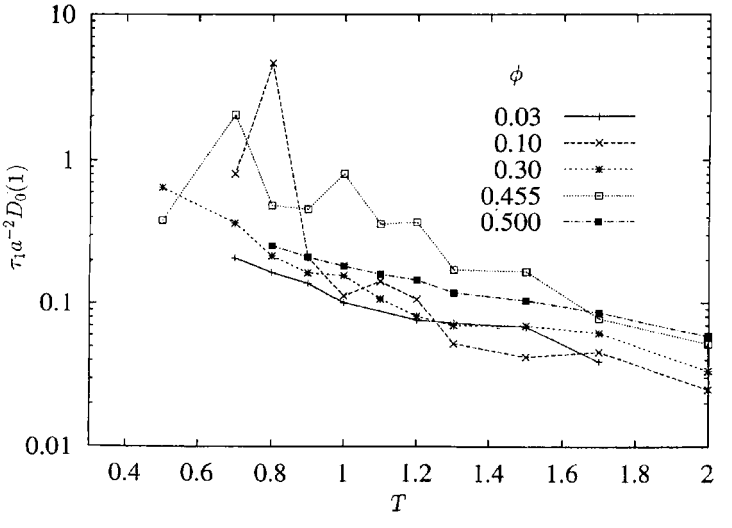

Figure 15 The longest relaxation time τ_1 as a function of temperature for the volume fractions indicated on the figure. $N = 108$.

magnitude larger than the τ_s at the same state point. This is because τ_s is a mean of all the component relaxation times in the system and therefore τ_s includes the shorter relaxation times as well as τ_1; all show evidence of increasing as temperature decreases.

The frequency dependent absolute complex viscosity, shown in Figure 16, gives another perspective on the critical slowing down of the dynamics through the quench. As expected, the greatest relative change with temperature is at low frequencies, as the modes of the network are most different from an unassociated fluid at low frequency. Figures 17 and 18 give the $\eta''(\omega)$ for $\phi = 0.33$ and 0.5, which manifest similar trends.

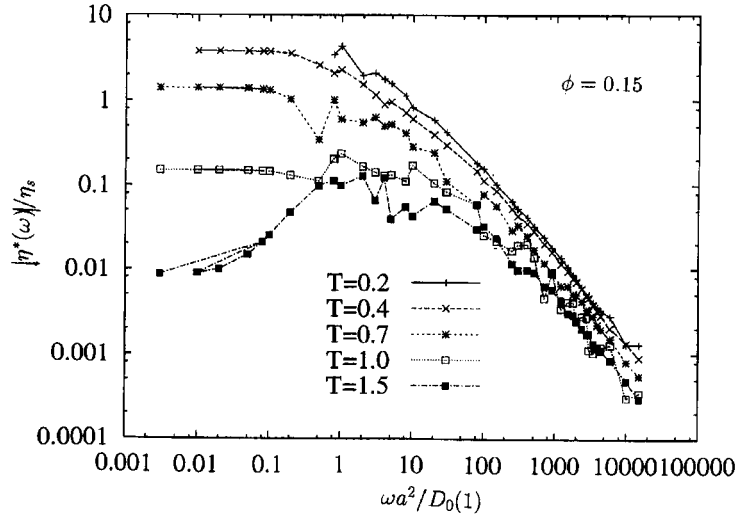

Figure 16 Complex viscosity for the states given on the figure. $N = 256$.

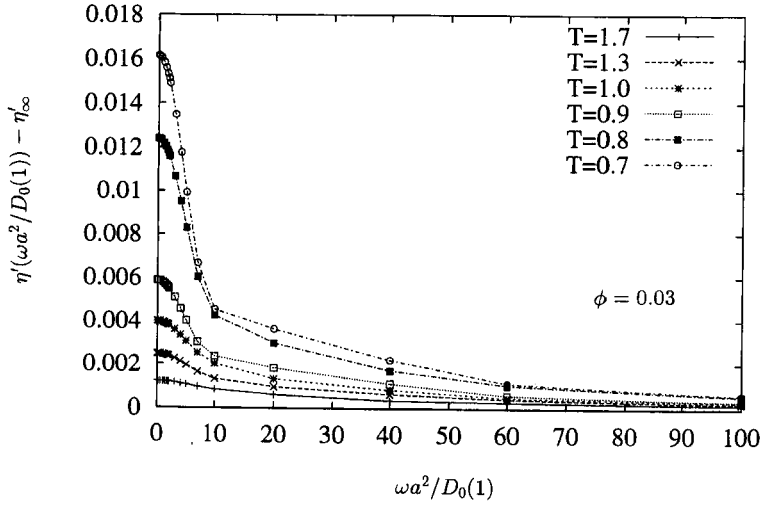

Figure 17 $\eta'(\omega)$ for $\phi = 0.03$ states at a series of temperatures. $N = 108$.

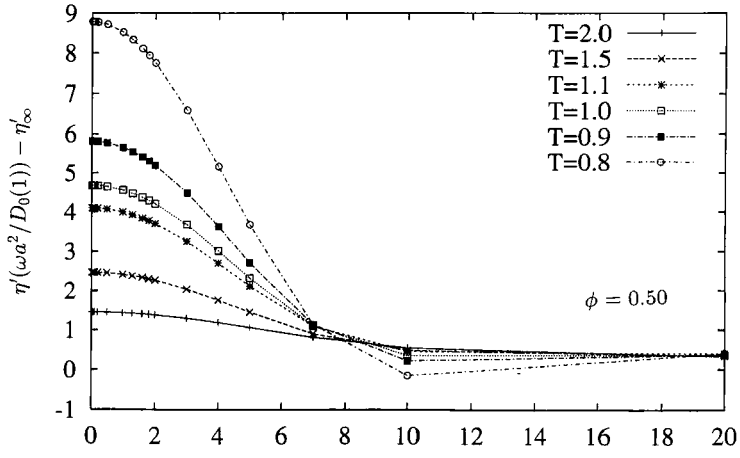

Figure 18 As for Figure 17, except $\phi = 0.5$.

Another perspective on these supercooled states is revealed in the structure factor, $S(k)$, which is obtained from the Fourier transform of the radial distribution function[27]. In Figure 19 are given $S(k)$ at different temperatures during the quench at $\phi = 0.314$. It is notable that $S(k)$ for $k \to 0$ diverges as temperature decreases, indicating an infinite compressibility [34], which is expected for a weak network. The enhanced tendency for network formation at low temperature, is also reflected in the percolation behaviour. We have computed the 'search diameter', σ_s, at which 50% of the computed configurations form percolating clusters, the so-called percolation

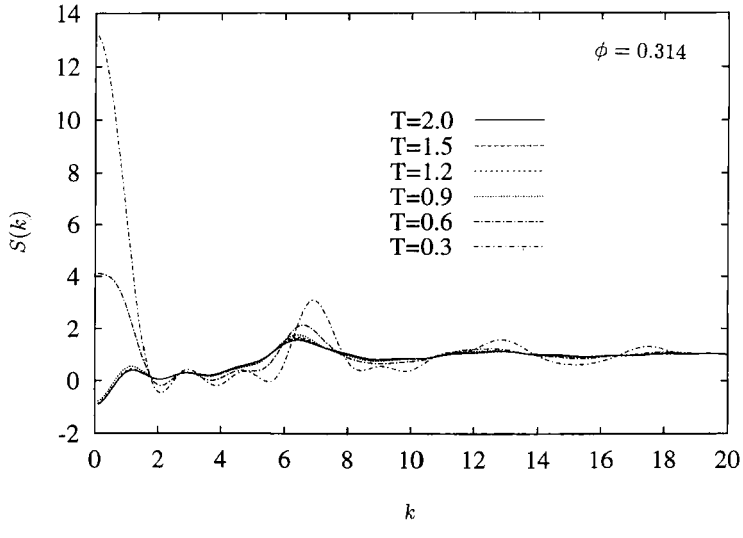

Figure 19 Structure factor for $\phi = 0.314$ states at different temperatures and for $N = 256$.

thereshold [35]. A particle is defined to belong to a cluster if its centre is within a distance of σ_s from the centre of at least one other particle already in the cluster. Table 2 shows that this distance decreases as temperature decreases, indicating that the system is becoming more 'connected'. At some large value of σ_s any system will percolate. The significance of a small value for σ_s is that the long-range structure in the system is facilitating network formation, so σ_s does not need to be so large.

4 CONCLUSIONS

We have used Brownian Dynamics to form a model particle gel by quenching a supercritical Lennard-Jones fluid in three dimensions well into the spinodal region of the phase diagram. At sufficiently low temperature (~ 0.3) a network does form which has a limiting diverging viscosity and zero self-diffusion coefficient and structural features associated with a classical gel. An optimum gel-like state would appear to form at a reduced number density of ~ 0.2, as this forms the sharpest transition, especially in thermodynamic properties. Also there is a critical number density of particles required to form a gel. For too many particles, the properties tend to show more gradual changes on cooling, more akin to a glass.

One of the main deficiencies in the current model is that, by having such large steps in the quench procedure we were unable to locate the gel point itself. This was reflected in our time correlation functions exhibiting stretched exponential, rather than algebraic decay with time, which is expected only at the gel point. Nevertheless, we have identified many of the features of classical sol-gel behaviour even with a simple Lennard-Jones model, auguring well for future studies of gels by Brownian Dynamics simulations.

Acknowledgements

JFL thanks the EPSRC for a research studentship.

References

1. M. J. Vold, *J. Coll. Sci.*, **18**, 684 (1963).
2. P. Meakin, *Phys. Rev. Lett.*, **51**, 1119 (1983).
3. R. Jullien, *Contemp. Phys.*, **28**, 477 (1987).
4. J. Liu, W. Y. Shih, M. Sarikaya and I. A. Aksay, *Phys. Rev., A*, **41**, 3206 (1990).
5. J. E. Martin, *Phys. Rev. A*, **36**, 3415 (1987).
6. J. E. Martin, J. Wilcoxon and J. Odinek, *Phys. Rev. A*, **43**, 858 (1991).
7. J. E. Martin and J. Wilcoxon, *Phys. Rev. Lett.*, **61**, 373 (1988).
8. M. Adam, M. Delsanti, J. P. Munch and D. Durand, *Phys. Rev. Lett.*, **61**, (1988).
9. D. F Hodgson and E. J. Amis, *Phys, Rev. A*, **41**, 1182 (1990).
10. M. Takahashi, K. Yokoyama, T. Masuda and T. Takigawa, *J. Chem. Phys.*, **101**, 798 (1994).
11. C. Michon, G. Cuvelier and B. Launay, *Rheolog. Acta.*, **32**, 94 (1993).
12. S. Z. Ren and C. M. Sorenson, *Phys. Rev. Lett.*, **70**, 1727 (1993).
13. G. Cuvelier, and B. Launey, *Makromol. Chem. Macromol. Symp.*, **40**, 23 (1990).
14. R.de Rooij, D. van den Ende, M. H.G. Duits and J. Mellema, *Phys. Rev. E*, **49**, 3038 (1994).
15. W.- H. Shih, W. Y. Shih, S. Il Kim, J. Liu and I. A. Aksay, *Phys. Rev. A*, **42**, 4772 (1990).
16. S. M. Ilett, A. Orrock W.C.K. Poon and P. N. Pusey, *Phys. Rev. E*, **51**, 1344 (1995).
17. W. C. K. Poon, A. D. Pirie and P. N. Pusey, *Faraday Disc.*, **101** (1995) in press.
18. D. A. Kofke, *J. Chem. Phys.*, **98**, 4149 (1993).

19. R. Agrawal and D. A. Kofke, *Mol. Phys.*, **85**, 43 (1995).
20. J. K. Johnson, J. A. Zollweg and K. E. Gubbins, *Mol. Phs.*, **78**, 591 (1993).
21. S. W. Koch, R. C. Desai and F. F. Abraham, *Phys. Rev., A*, **27**, 2152 (1983).
22. B. D. Butler, H. J. M. Hanley, D. Hansen and D. J. Evans, *Phys. Rev. Lett.*, **74**, 4468 (1995).
23. E. Valasco, and S. Toxvaerd, *Phys. Rev. Lett.*, **71**, 388 (1993).
24. M. R. Mruzik, F. F. Abraham and G. M. Pound, *J. Chem. Phys.*, **69**, 3462 (1978).
25. R. Zwanzig and R. D. Mountain, *J. Chem. Phys.*, **43**, 4464 (1965).
26. T. Akesson and B. Jönsson, *Molec. Phys.*, **54**, 369 (1985).
27. P. J. Mitchell, D. M. Heyes and J. R. Melrose, *JCS Farad. Trans.*, **91**, 1975 (1995).
28. C. P. Lindsey and G. D. Patterson, *J. Chem. Phys.*, **73**, 3348 (1980).
29. D. M. Heyes and P. J. Mitchell, *JCS Farad. Trans.*, **90**, 1931 (1994).
30. J. H. R Clarke, *JCS Farad.*, II **75**, 1371 (1979).
31. L. V. Woodcock, *Mol. Sim.*, **2**, 253 (1989).
32. A. J. Hopkins and L. V. Woodcock, *JCS Farad. Trans.*, **86**, 2121 (1990).
33. J. C. van der Werff, C. G. de Kriuf, C. Blom and J. Mellema, *Phys. Rev. A*, **39**, 795 (1989).
34. J. P. Hansen and I. R. McDonald, 'Theory of Simple Liquids' Academic press, 2nd Edition, page 99.
35. D. M. Heyes and J. R. Melrose, *Mol. Phys.*, **66**, 1057 (1989).

APPENDIX A

The program units (denoted by*) for length (L), mass (M) and energy (E) are $L^* = L/\sigma$, $M^* = M/m$ and $E^* = E/\varepsilon$ where σ and ε are defined in the pair potential of Eqn. (1). Mass, m is the mass of the colloidal particle. The mass of the colloidal particle plays no role in the dynamics of large colloidal particles, the so-called 'creeping flow' limit. Nevertheless it is still a useful internal unit or intermediate unit within the BD program.

The scaling behaviour of suspension rheology has been a subject of considerable interest [31] [32]. Dispersion rheology for suspended particles of arbitrary diameter and solvent viscosity can be reduced in the low Reynolds number limit (i.e., where suspended particle inertia can be ignored) as follows. The shear rate, $\dot{\gamma}$, scales as the Peclet number, $P_e = \dot{\gamma}\tau$ where $\tau = a^2/D_0$, for a spherical particle of radius, a. D_0 is the self-diffusion coefficient of the particle at infinite dilution. τ is the natural unit of time, as it has the size and solvent dependence of structural relaxation behaviour included in its definition. The infinite dilution value for the self-diffusion coefficient, $D_0(T) = k_B T/\zeta_0$ and the friction coefficient, $\zeta_0 = 3\pi\sigma\eta_s$ where η_s is the viscosity of the solvent. This scaling behaviour enables the computations to be carried out without specifying an explicit σ or η_s.

In program units, $\zeta_0^* = 3\pi\sigma^*\eta_s^* = 3\pi\eta_s^*$, as $\sigma^* = 1$. It is convenient to arrange that $\zeta_0^* = 1$, which forces the definition, $\eta_s^* = 1/3\pi$. Therefore in the computer program, the solvent viscosity has the numerical value of $1/3\pi$.

The infinite dilution value for the self-diffusion coefficient, $D_0^*(T) = k_B T/\xi_0^*$ and in program units, $D_0^*(T) = k_B T/\zeta_0^* = T^*$. Therefore, $D_0^*(T^* = 1) = D_0^*(1) = 1$. From this the reference reduced relaxation time can be defined as $\tau = a^2/D_0(1)$. We have $\tau^* = a^{*2}/D_0^*(1) = 1/4$. The particle-based unit for time is $\sigma(m/\varepsilon)^{1/2}$ and therefore $\tau = 4^{-1}\sigma(m/\varepsilon)^{1/2}$. An alternative reduced time and self-diffusion coefficient would be to scale out the temperature as well, i.e., $\tau^*(T) = a^{*2}/D_0^*(T^*) = T^*/4$. We use both definitions. The former definition is temperature independent, whereas the latter scales out the 'trivial' temperature dependence of a property that arises by virtue of

the change in mobility of the individual particles. (Note that in the model, the mean square displacement in a time step from the Brownian motion component of the dynamics, $\langle \Delta r^2(\Delta t) \rangle = 6D_0 \Delta t$.) Generally, it is not meaningful to use $\tau^*(T)$ for unit of time, especially if states at different temperature are being considered, as in the present study. It is better to use $\tau = a^2/D_0(1)$ as the unit of time. However, $D(t)/D_0^*(T)$ is a sensible reduction of the time dependent self-diffusion coefficients, as discussed in the main text.